Strain-induced ferromagnetism in zigzag edge graphene nanoribbon with a topological line defect

Ting Hu,[1] Jian Zhou,[2] Jinming Dong,[1,*] and Yoshiyuki Kawazoe[3]

[1]*Group of Computational Condensed Matter Physics, National Laboratory of Solid State Microstructures and Department of Physics, Nanjing University, Nanjing 210093, P. R. China*

[2]*Department of Materials Science and Engineering, Nanjing University, Nanjing 210093, P. R. China*

[3]*Institute for Materials Research, Tohoku University, 2-1-1 Katahira Aoba-ku, Sendai, 980-8577 Japan*

(Received 18 June 2012; published 12 September 2012)

The electronic and magnetic properties of the zigzag edge graphene nanoribbon with a topological line defect (LD-ZGNR) have been studied under an external strain along ribbon axis by using first-principle calculations. It is found that the applied strain induces the local magnetic moments on the line defect, whose coupling with those on the edges leads to a turnover of the spin polarization on one edge, making the LD-ZGNR become a ferromagnetic (FM) metal at a large enough strain. When the strain increases to larger than 16%, a transition from a FM metal to a FM semiconductor will happen. Our calculation results suggest a possible way to tune the magnetic and transport properties of the LD-ZGNR by applying the strain, which is very useful for applications of the graphene ribbon in spintronics and electromechanical devices.

DOI: 10.1103/PhysRevB.86.125420 PACS number(s): 73.22.−f, 75.75.−c, 71.55.−i, 71.15.Mb

I. INTRODUCTION

Graphene, an important two-dimensional carbon allotrope, has been a hot topic in recent years due to its extraordinary mechanical, electronic,[1] optical, and magnetic[2] properties. Both the graphene and the quasi-one-dimensional (Q1D) graphene nanoribbons (GNRs) have been extensively investigated in theoretical and experimental works.[3–9] In particular, the GNR's magnetism has attracted great interest since its promising applications in the design of nanoscale magnetic and spintronics devices.[10,11] It has been shown that the GNRs with zigzag edges (ZGNRs) are characterized with special localized edge states, showing a ferromagnetic (FM) order in the same edge but antiferromagnetic (AFM) order between two opposite edges.[12–14]

In addition, the FM ordering has been found to also exist in graphene materials with defects, such as vacancies, topological defects, edges, and hydrogen chemisorptions.[15–18] Recently, a new type of topological line defect in graphene, composed of octagonal and pentagonal sp^2-hybridized carbon rings, has been observed, which is found to be a metallic wire.[19] The line defect divides a graphene sheet into two domains, both of which have the zigzag crystallographic directions along the line defect. Furthermore, it has been found theoretically that when the line defect is introduced into a ZGNR, the localized states on the line defect would affect its magnetic behavior. For example, when the line defect position changes, a transition from an AFM semiconductor to an AFM half-metal will appear.[20]

On the other hand, graphene has been confirmed mechanically as a strong material, which is able to sustain reversible elastic deformations in excess of 20%.[21] Moreover, it has been shown that an applied strain could be a useful way to further tailor the graphene's electronic and magnetic properties.[22–25] In particular, a strain along the graphene's zigzag direction might eventually lead to a gap opening at large deformations.[23] A recent theoretical work has shown that the tensile strain along the zigzag direction of graphene with topological line defects can greatly enhance the local magnetic moments on the line defects.[26]

In this paper, we have studied the ZGNR with a topological line defect at its middle (LD-ZGNR), parallel to its edges, and suffering a tensile strain along the line defect by using first-principles calculations. It has been found that the tensile strain could induce the local magnetic moments on the line defect, leading to a magnetic transition for the LD-ZGNR from the initial AFM state to the FM one under a large enough tensile strain, in which the spin moments on its two edges become parallel from originally being antiparallel.

The remainder of this paper is organized as follows. In Sec. II, the geometrical structure of LD-ZGNR and computational details are described. In Sec. III, the main numerical results and some discussions are given. Finally, in Sec. IV, a conclusion is presented.

II. MODEL AND METHOD

The optimized geometric structure of the LD-ZGNR is shown in Fig. 1, which is still a Q1D periodic system along its axis direction even though it has a line defect. It is known from Fig. 1 that the line defect in a unit cell of the LD-ZGNR is composed of one octagonal and a pair of pentagonal sp^2-hybridized carbon rings. And a line defect separates a ZGNR into two parts with zigzag edges, which can be denoted as the left and right ribbons. Thus, we can use a symbol of $N1$-$N2$-LD-ZGNR to mark the zigzag edge GNRs with a line defect, where $N1$ and $N2$ represent the numbers of zigzag chains in its left and right ribbons, respectively. For simplicity, however, we only study in this paper a simple case of $N1 = N2 = N$ because the position of the line defect in the ZGNR has a big effect on its magnetic properties.[20]

The geometric, electronic, and magnetic properties are calculated using the spin polarized density functional theory in the generalized gradient approximation (GGA), implemented by the Vienna *Ab initio*_Simulation_Package (VASP),[27,28] in which the projected augmented wave method[29] and the Perdew–Burke–Ernzerhof (PBE)[30] exchange-correlation functional are employed. The $2s$ and $2p$ orbitals of the carbon atom are treated as valence ones. A large supercell along the width direction of the LD-ZGNR is used to simulate the

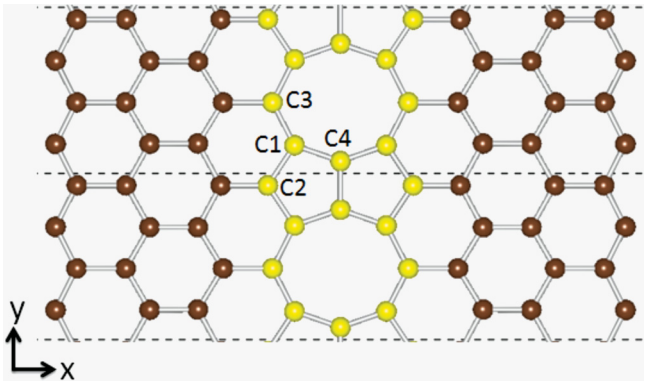

FIG. 1. (Color online) The optimized geometrical structure of a 3-3-LD-ZGNR, where the carbon atoms on the line defect are represented by yellow (light gray). The line defect in each unit cell has 10 carbon atoms, which are divided into four types, C1, C2, C3, C4, based upon the structure symmetry.

isolated Q1D LD-ZGNR, making the closest distance between two adjacent LD-ZGNRs 15Å. The ribbon is placed along the y direction, and large vacuum volume region is added in both x and z directions.

Geometric structures of the LD-ZGNRs are optimized by the conjugated-gradient minimization scheme. A plane-wave cutoff of 520 eV was used in our simulations, and the energies were converged to 10^{-5} eV/atom. Both the atomic positions and the lattice constant along the ribbon axis are fully relaxed until the maximum residual forces on atoms were less than 0.005 eV/Å. The 1D Brillouin integration was sampled with a $1 \times 10 \times 1$ Monkhorst–Pack grid.

III. RESULTS AND DISCUSSIONS

A. Variation of magnetic properties with an applied tensile strain

We first studied the electronic structure and magnetic property of the N-N-LD-ZGNR without an applied strain by first-principles calculations. It is found that in this case its ground state is the same as that of the conventional ZGNR without the line defect, i.e., the magnetic moments mainly localize on the two zigzag edges, which are FM coupling in the same zigzag edges but AFM between the two opposite zigzag edges. There are only negligible magnetic moments within the line defect region.

Then an external tensile strain is applied on the LD-ZGNR along its edge direction, whose width shrinkage in its edge-normal direction due to the Poisson's ratio effect is automatically taken into account in the calculations. Taking 3-3-LD-ZGNR as an example, we have calculated its electronic structures and magnetic properties under different tensile strains. The calculated spin polarized charge densities ($\rho_{up} - \rho_{down}$) of the 3-3-LD-ZGNR under two different strains (0% and 5%) are shown in Figs. 2(a) and 2(b), respectively, where the ρ_{up} and ρ_{down} denote the spin-up and spin-down electron densities, respectively. The spin polarized charge densities of the 3-3-LD-ZGNR under other strains have been also calculated, which are found to be similar either to those at zero strain if the applied strain is smaller (e.g., under a 1% strain) or to those under a 5% strain if the applied strain becomes larger (e.g., under the strains from 2% to 20%).

It is seen clearly from Fig. 2 that the ground state of 3-3-LD-ZGNR under a 0% strain is AFM coupling between its two edges with negligible magnetic moments in the line defect region. However, the magnetic moments of the line defect are enhanced under a 5% strain, and the AFM couplings between the magnetic moments on the line defect and edges become strong enough to turn over the spin polarization direction of one edge, which causes the large magnetic moments on its two edges to point to the same direction but the small ones on the line defect to point to the opposite direction, finally leading to a FM 3-3-LD-ZGNR.

The calculated results on the magnetic moment variation of 3-3-LD-ZGNR with the applied strains are given in Fig. 3(a). The maximum strain we applied is 20%, which is still within the range of the graphene's elastic limit and, therefore, the modulation of magnetism is fully reversible. It is seen from Fig. 3(a) that the total magnetic moments of 3-3-LD-ZGNR are enhanced by the external strain in a large range. At 0% and a small 1% strain, the ribbon's total magnetic moment keeps 0 μ_B, indicating the spin configuration of the system is still in the AFM state. When the applied strain increases to 2%, the total magnetic moment per unit cell sharply increases to about 5 μ_B and then slowly increases to about 6 μ_B as the strain increases to 20%. That is because at an applied strain larger than 2%, the spin polarizations on the two edges turn to the same direction due to their AFM couplings with those on

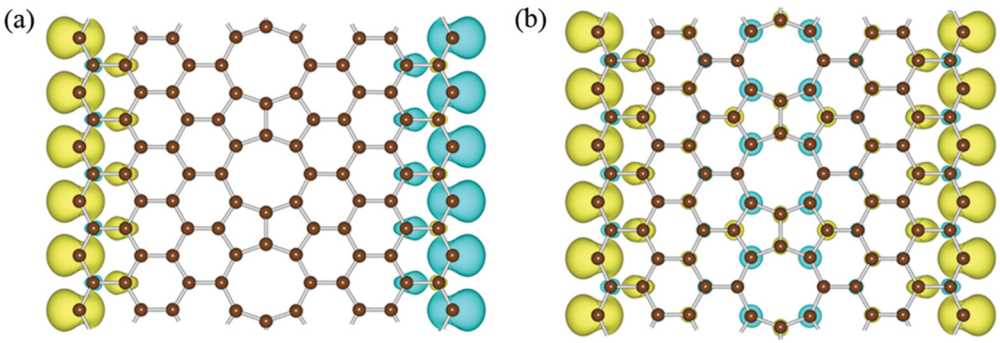

FIG. 2. (Color online) Spin polarized charge density ($\rho_{up} - \rho_{down}$) of 3-3-LD-ZGNR under applied tensile strains of (a) 0% and (b) 5%. Here, the ρ_{up} and ρ_{down} denote the spin-up and spin-down electron densities, represented by the yellow (light gray) and cyan (medium gray) colors, respectively.

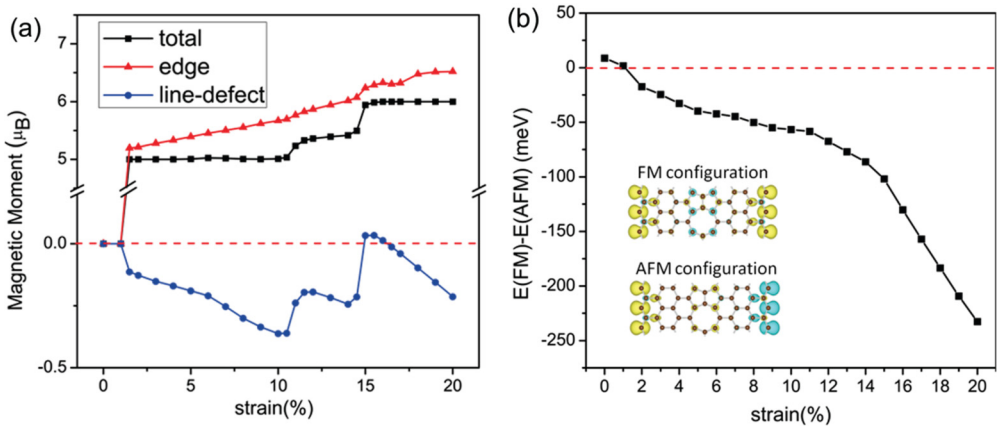

FIG. 3. (Color online) The 3-3-LD-ZGNR in one unit cell. (a) The total magnetic moment (black line), the magnetic moment summed over four edge atoms and their next-nearest neighbor ones (red line) and that integrated over the line defects (blue line) versus the applied strain. Here, the positive and negative values indicate the corresponding spin polarizations are spin-up and spin-down, respectively. The red dashed line represents the zero magnetic moment. (b) The energy difference ($\Delta E = E_{\mathrm{FM}} - E_{\mathrm{AFM}}$) between its FM and AFM configurations varying with the strain, where the red dashed line represents the zero energy difference. Inserts in (b) represent the FM and AFM configurations, respectively.

the line defect, making the large magnetic moments on its two edges parallel but the small ones on the line defect antiparallel to them, which finally leads to FM 3-3-LD-ZGNR.

The energy difference ($\Delta E = E_{\mathrm{FM}} - E_{\mathrm{AFM}}$) per unit cell between the FM and AFM configurations of 3-3-LD-ZGNR, varying with applied strain, is given in Fig. 3(b). Here, the spin polarization at the left edge is defined as spin-up. Then the polarization at the right edge should be spin-up or spin-down in the FM or AFM states, respectively. As for the spin polarization on the line defect, it is found that in the FM state, it is spin-down, coupling antiferromagnetically with those on two edges. While in the AFM state, the two cases with its spin being up or down are energy degenerate; therefore, we can accept either one of them. In Fig. 3(b), it is taken as spin-up. It is obviously seen from Fig. 3(b) that at 0% and a small strain of 1% the ΔE is positive, indicating the AFM state is more stable than the FM one. As the strain reaches 2%, the ΔE becomes negative, indicating that the FM state becomes more stable than the AFM one, which is consistent with the sudden increase of the total magnetic moment under a 2% strain. Moreover, the ΔE monotonically decreases as the strain increases, indicating the stability of the FM state increases with increasing the external strain.

Now we would like to explain more clearly the intuitive physics on the transition of AFM to FM ordering under a tensile strain, obtained previously. The clearer picture on it is given as follows. (1) Under no strain, the LD-ZGNR is in the AFM ground state, in which the magnetic moments localized on its two edges are FM coupling along the same edge but are AFM coupling between its two opposite edges, as seen from Figs. 2(a) and 3(b). (2) Under an applied strain, the new magnetic moments appear on the line defects, increasing with the applied strain, which are found in the AFM couplings with those on the two edges, as seen from Fig. 2(b). (3) Thus, under a large enough strain (e.g., >2%), the magnetic moments on the line defects become large enough, which are able to turn the antiparallel spin polarizations on the two edges parallel because of the AFM couplings between the magnetic moments on the two edges and the line defects, leading to the transition of the original AFM ordering into the final FM ordering, as seen from Figs. 2(b) and 3.

Therefore, the appearance of new magnetic moments on the topological line defects under an applied strain is the key point of inducing the AFM to FM transition under a tensile strain. This mechanism also explains why the existence of the topological line defect in the ZGNR is necessary for the occurrence of the AFM to FM transition under the tensile strain because without the line defect, the strain would not be able to induce the new magnetic moments in the interior of ZGNR, which can only increase the band gap but maintain its AFM ground state.[31] Thus, in this case, an applied tensile strain would not cause the reversal of the spin polarization on one edge of ZGNR and would not induce the transition of an AFM state to a FM one.

To give a detailed analysis of the dependence of the system's magnetic properties on the external strain, we have calculated the absolute value of local magnetic moments at the edge atoms and the line defect atoms by using the Bader charge analysis.[32] It is found that the total magnetic moment of the FM state is mainly contributed by the four edge atoms and their next-nearest neighbor ones in a unit cell, called magnetic moment on the edges, while the atoms on the line defect have a small and negative contribution, as shown in Fig. 3(a). It is seen obviously from Fig. 3(a) that the magnetic moment on the edges increases almost linearly from 5.21 to 6.52 μ_{B} as the strain increases from 2% to 20%, while the magnetic moment, contributed by all the atoms on the line defect, displays an oscillating behavior when increasing the strain, in which the negative value indicates its polarization is spin-down. The increase of both the magnetic moments with opposite spin polarizations on the edges and the line defect causes their summation, i.e., the total magnetic moment in one unit cell, to keep the 5 μ_{B} under the strain varying from 2% to 10%. After that, due to the jump decrease of the magnetic moment on the line defect at the strain of 10% and 15%, the total magnetic moment exhibits an

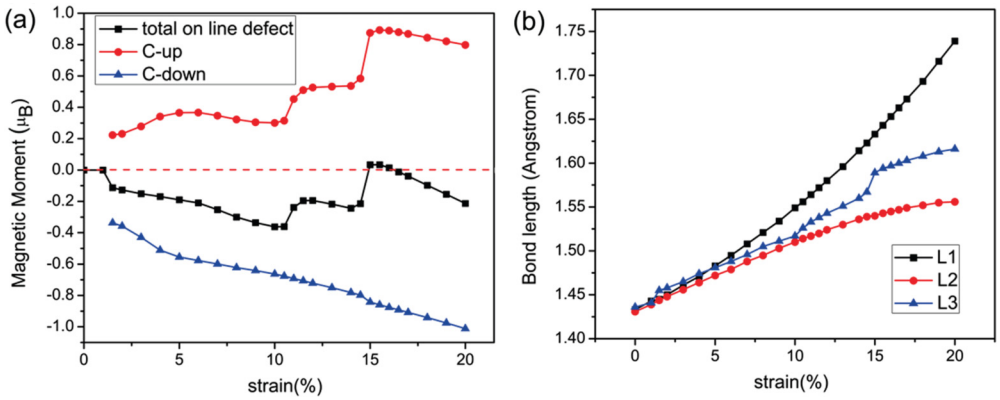

FIG. 4. (Color online) The 3-3-LD-ZGNR in one unit cell. (a) The total magnetic moment on its line defect and the corresponding local magnetic moments on the C-up (i.e., C2, C3, C4-type) and C-down (C1-type) carbon atoms versus the external strain. (b) The bond length variation of three key bonds versus the external strain. Definitions of $L1$, $L2$, and $L3$ are given in the inset.

increase in stair-step and finally increases to about 6 μ_B under the strain of 15% to 20%.

Since the local magnetic moment integrated over the line defect can be viewed as a summation of those on four types of line defect atoms, C1, C2, C3, and C4, we can examine the local magnetic moments on them separately. The spin polarizations on four C1-type atoms are found to be spin-down, and those on C2, C3, C4-type atoms are spin-up. Thus, we will define the C1-type atoms as the C-down atoms and all the C2, C3, C4-type atoms as the C-up ones. The absolute value of local magnetic moment on those C-down atoms is found to be enhanced almost linearly by the external strain, while those on all the C-up atoms exhibit stair-type rises, as shown in Fig. 4(a). The total magnetic moment on the line defect is found to be mainly contributed by the C-down atoms when the applied strain increases from 2% to 10%, exhibiting an absolute value increase with the strain. But, when the strain increases from 11% to 20%, those spin-up magnetic moments on all the C-up atoms are enhanced greatly, showing two step rises under the strain of 10% and 15% and presenting thus a big contribution to the oscillating behavior of the magnetic moment localized on the line defects.

Because the magnetic moment is closely related to the bond length, we have calculated the variations of the related bond lengths with external strain for the four types of carbon atoms on the line defects. Due to the Poisson's ratio effect, the bonds mainly along the edge direction are elongated largely under the tensile strains, while those mainly perpendicular to the edge direction are slightly shortened, which causes the former to play a major role in the variation of the local magnetic moment on the line defect with applied strain. The response of three key bonds $L1$, $L2$, and $L3$ to the external strain is given in Fig. 4(b), from which we can find that the bond lengths $L1$ and $L2$ increase monotonically with strain, which thus leads to an increase of the average distance between two C1 atoms and finally an almost linear increase of the absolute value of local magnetic moment on the C1 atoms. Meanwhile, the jump-type increase of the $L3$ bond length at the strain of 10% and 15% is responsible for the stair-type rise of the magnetic moment on C-up atoms.

B. Electronic band structure

To interpret the origin of the magnetic moments localized on the line defect, we have calculated the spin polarized band structures of the 3-3-LD-ZGNR under different strains of 0%, 2%, 9%, 11%, 14%, and 16%, which are given in Figs. 5(a) to 5(f), respectively, where the spin-up and spin-down bands are denoted by the black and red (dark gray) lines, respectively. As mentioned previously, the 3-3-LD-ZGNR without strain is in the AFM state, in which the spin-up and spin-down bands are degenerate with an indirect band gap of about 0.15 eV. And there are two flat bands near the Fermi level, labeled as a and b, which are marked by black triangles and green (gray) inverted triangles, respectively, as shown in Fig. 5(a). As the strain increases to 2%, these two flat bands near the Fermi level become spin split.

For further analysis, we also calculated the projected densities of states (pDOS) of the system at 2% strain in the FM state for p orbitals of the edge atoms and p_z orbitals of all the carbon atoms on the line defect, which are given on the left and right sides of the band structure, shown in Fig. 5(b). It can be seen from the pDOSs that the flat bands (both a and b) near the Fermi level are mainly contributed by the π bonds on the line defect. Besides, there is a spin-up band crossing the Fermi level with its occupied part contributed mainly by the p_z orbitals of the edge atoms, which is labeled as c and marked by the blue (medium gray) dots in Figs. 5(b) to 5(f). Moreover, the dangling bond energy levels are found to lie in the energy range of about -3 to -1 eV of its valence band of spin-up channel, as indicated by the red (dark gray) dots in Fig. 5, which exhibit the p_y character in the pDOS of the edge atoms.

Furthermore, with the increase of external strain, the spin splitting is enhanced gradually. It can be found from Figs. 5(b) to 5(f) that the spin-down a band descends and the spin-down b band ascends, while the spin-up b band first rises as the strain varies from 2% to 10% and then falls when the strain further increases from 11% to 15%, leading to the oscillating behavior of magnetic moment on the line defect. Moreover, the spin-up c band gradually descends as the strain increase, indicating an increase of the orbital occupation of edge atoms, which leads to the increase of magnetic moment on the edges.

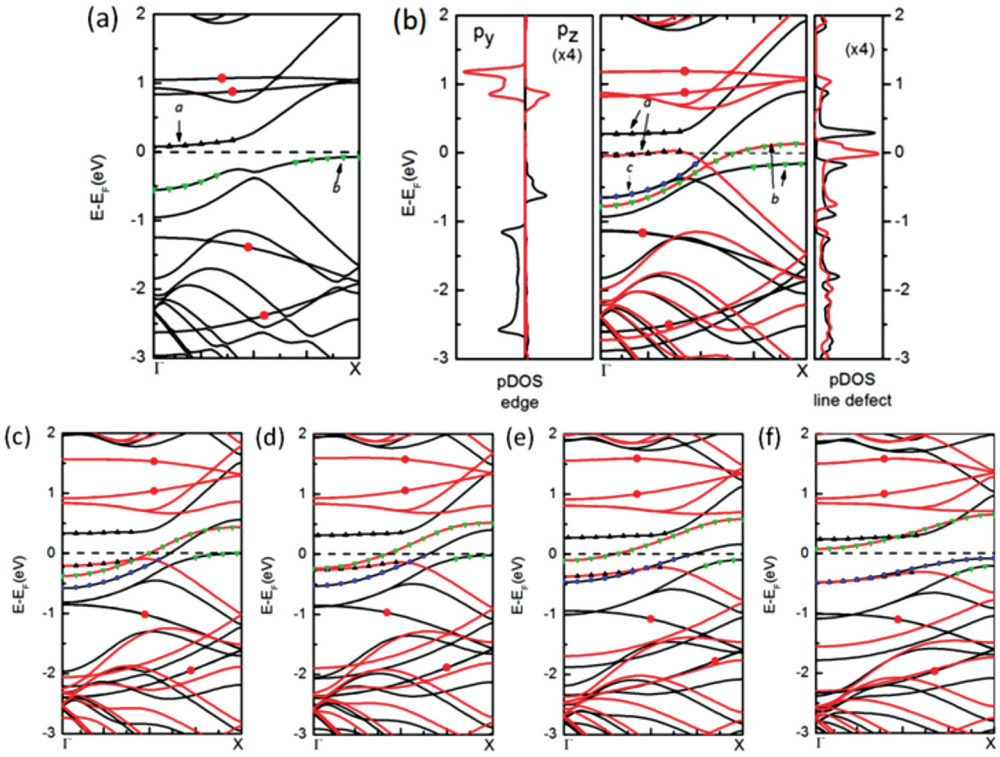

FIG. 5. (Color online) The spin polarized band structures of the 3-3-LD-ZGNR in a unit cell under different strains: (a) 0%, (b) 2%, (c) 9%, (d) 11%, (e) 14%, (f) 16%. The pDOS for the p_y and p_z of four edge atoms is shown on the left-hand side of the band structure. And the pDOS summed over the π orbitals of all the line defect atoms is given on the right-hand side of the band structure, which is magnified by four times in the figure. The black and red (dark gray) lines denote the spin-up and spin-down states in both the band structures and pDOSs, respectively. The red (dark gray) circles represent the dangling bonds.

Notably, when the strain increases to 16%, it is seen from Fig. 5(f) that now there are no bands crossing the Fermi level, making the system a semiconductor with an indirect band gap of about 0.16 eV, which increases with the external strain. Thus, the total magnetic moment of the system keeps 6 μ_B when the strain increases from 16% to 20%.

We would like to emphasize that up to now, for simplicity, our calculations have been made for the LD-ZGNR with naked zigzag edges (i.e., without hydrogen termination). One might be concerned about the effect of the hydrogen termination, which greatly stabilizes the ZGNR in practice, on the previous calculation results of the LD-ZGNR, especially the AFM to FM transition. In order to address this concern, we have also studied the 3-3-LD-ZGNR with H termination under no strain and 5% strain.

It is found that the dangling bonds are indeed removed after the H termination. Thus the local spin moments of 3-3-LD-ZGNR under no strain are reduced greatly from 1.2 μ_B per atom at the naked edges to 0.2 μ_B at the H-terminated ones, which are still FM coupling in the same H-terminated edges but AFM coupling between two opposite H-terminated ones. More importantly, it is found that under 5% strain, the local spin moments still appear on the line defects, as in the case without H termination, which causes the energy difference ΔE between the FM and AFM states of the 3-3-LD-ZGNR with H termination to vary from 9 to -16 meV, indicating a strain-induced transition from the AFM state to the FM state, even though the dangling bonds at the zigzag edges are removed by the H termination. The total magnetic moment of the 3-3-LD-ZGNR with H termination is found to be 1 μ_B in one unit cell, in contrast to 5 μ_B in the case without H termination. Therefore, the H termination, happening frequently in practice and greatly stabilizing the zigzag edge structure, will not change qualitatively the main results obtained in our paper.

C. Dependence of magnetic properties on the ribbon width

Now, it is interesting to find the dependence of both the total magnetic moment and the FM state stability on the ribbon's width. Thus, we have explored how the energy difference ΔE between the FM and AFM states varies with the LD-ZGNR's width under a certain external strain (10% for instance). The obtained results are given in Fig. 6(a), from which it is seen clearly that the energy difference ΔE is always negative, indicating that the FM configuration is more stable than the AFM one when the width increases from $N = 1$ to 8. Moreover, the absolute value of ΔE decreases as the width increases and might eventually vanish at a very large ribbon width. It is found that at the width of $N = 6$, corresponding to about 30 Å, the $\Delta E \approx 25$ meV, indicating the LD-ZGNR could still have room temperature magnetic ordering at this rather large width, which is much larger than that ($\backsim$10 Å) of the pristine ZGNRs at about the same energy difference. Thus, it is easier to use such LD-ZGNR in the spintronic devices operating at room temperature.[33]

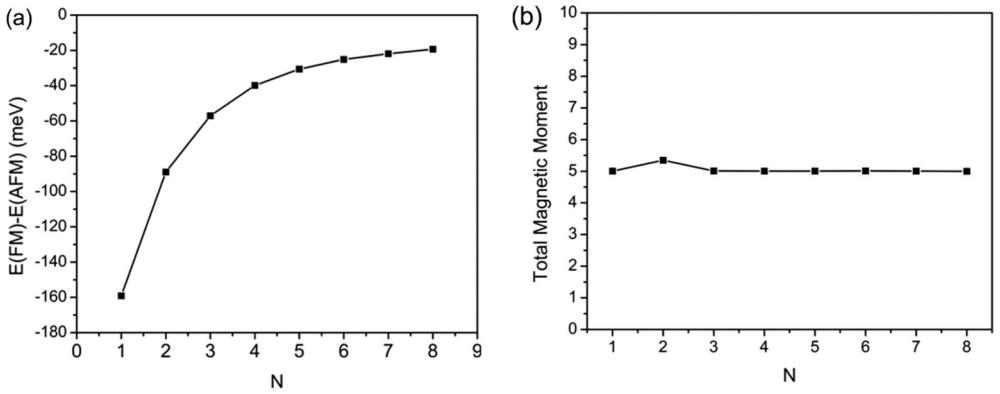

FIG. 6. A N-N-LD-ZGNR under a fixed external strain of 10%. (a) The energy difference $\Delta E = E_{\mathrm{FM}} - E_{\mathrm{AFM}}$ per unit cell between its FM and AFM configurations varies with ribbon's width, denoted here by the index N. (b) Its total magnetic moment per unit cell versus the ribbon's width.

In addition, the calculated total magnetic moment per unit cell as a function of ribbon's width is shown in Fig. 6(b), indicating that its value remains almost unchanged at a value of about 5 μ_{B} as the width increases.

IV. CONCLUSIONS

The electronic structures and magnetic properties of the naked ZGNRs with topological line defects (LD-ZGNRs) lying symmetrically on the ribbon's middle have been studied under an external tensile strain along the edge direction by using first-principles calculations. It is found that the ground state of unstrained LD-ZGNRs is the AFM one, in which the magnetic moment localized on the line defect is negligible. When an external tensile strain is applied along the edge direction, the energy bands near the Fermi level would be spin-split, which are mainly contributed by the π orbitals on the line defect atoms. The band splitting is enhanced with increasing the strain, leading to an increase of the local magnetic moments on the line defect. Thus, the AFM coupling between the magnetic moments on the edges and line defects eventually leads to a turnover of spin polarization direction on one edge at a critical value of the tensile strain, causing the LD-ZGNR to be FM. A detailed calculation on the variation of the local magnetic moments and the spin polarized electronic structures of the LD-ZGNR with the applied strain reveals a possibility to tune the electronic and magnetic properties of the LD-ZGNR by an applied strain, which would cause the LD-ZGNR to be used in future spintronics devices and electromechanical ones. Besides, the H termination, stabilizing greatly the zigzag edge structure, is found not to change qualitatively the obtained main results.

ACKNOWLEDGMENTS

This work is supported by the National Natural Science Foundation of China under Grant Nos. 10874067 and 11004094. We also acknowledge the support from the State Key Program for Basic Research of China through the Grant Nos. 2010CB630704 and 2011CB922100Q. Our density functional theory calculations were performed in the High Performance Computing Center of Nanjing University.

*Corresponding author: jdong@nju.edu.cn

[1] A. H. C. Neto, F. Guinea, N. M. R. Peres, K. S. Novoselov, and A. K. Geim, Rev. Mod. Phys. **81**, 109 (2009).
[2] E. J. Kan, Z. Y. Li, and J. L. Yang, Nano **3**, 433 (2009).
[3] K. Nakada, M. Fujita, G. Dresselhaus, and M. S. Dresselhaus, Phys. Rev. B **54**, 17954 (1996).
[4] K. Wakabayashi, M. Fujita, H. Ajiki, and M. Sigrist, Phys. Rev. B **59**, 8271 (1999).
[5] T. Kawai, Y. Miyamoto, O. Sugino, and Y. Koga, Phys. Rev. B **62**, R16349 (2000).
[6] K. Tada and K. Watanabe, Phys. Rev. Lett. **88**, 127601 (2002).
[7] T. Matsui, H. Kambara, Y. Niimi, K. Tagami, M. Tsukada, and H. Fukuyama, Phys. Rev. Lett. **94**, 226403 (2005).
[8] K. Sasaki, S. Murakami, and R. Saito, J. Phys. Soc. Jpn. **75**, 074713 (2006).
[9] S. Dutta and S. K. Pati, Carbon **48**, 4409 (2010).
[10] P. Blake, P. D. Brimicombe, R. R. Nair, T. J. Booth, D. Jiang, F. Schedin, L. A. Ponomarenko, S. V. Morozov, H. F. Gleeson, E. W. Hill *et al.*, Nano Lett. **8**, 1704 (2008).
[11] W. Y. Kim and K. S. Kim, Nat. Nanotechnol. **3**, 408 (2008).
[12] S. M. Ryu, M. Y. Han, J. Maultzsch, T. F. Heinz, P. Kim, M. L. Steigerwald, and L. E. Brus, Nano Lett. **8**, 4597 (2008).
[13] Y. W. Son, M. L. Cohen, and S. G. Louie, Phys. Rev. Lett. **97**, 216803 (2006).
[14] Y. Li, Z. Zhou, P. Shen, and Z. Chen, J. Phys. Chem. C **113**, 33 (2009).
[15] K. H. Han, D. Spemann, P. Esquinazi, R. Höhne, V. Riede, and T. Butz, Adv. Mater. **15**, 1719 (2003).
[16] M. A. H. Vozmediano, M. P. Lopez-Sancho, T. Stauber, and F. Guinea, Phys. Rev. B **72**, 155121 (2005).
[17] O. V. Yazyev and L. Helm, Phys. Rev. B **75**, 125408 (2007).

[18]S. Okada, K. Nakada, K. Kuwabara, K. Daigoku, and T. Kawai, Phys. Rev. B **74**, 121412 (2006).
[19]J. Lahiri, Y. Lin, P. Bozkurt, I. I. Oleynik, and M. Batzill, Nature Nanotech. **5**, 326 (2010).
[20]X. Lin and J. Ni, Phys. Rev. B **84**, 075461 (2011).
[21]F. Liu, P. Ming, and J. Li, Phys. Rev. B **76**, 064120 (2007).
[22]S. M. Choi, S. H. Jhi, and Y. W. Son, Phys. Rev. B **81**, 081407 (2010).
[23]V. M. Pereira, A. H. Castro Neto, and N. M. R. Peres, Phys. Rev. B **80**, 045401 (2009).
[24]M. Fujita, K. Wakabayashi, and K. Nakada, J. Phys. Soc. Jpn. **65**, 1920 (1996).
[25]Y. Lu and J. Guo, Nano Res. **3**, 189 (2010).
[26]L. Kou, C. Tang, W. Guo, and C. Chen, ACS Nano. **5**, 1012 (2011).
[27]G. Kresse and J. Hafner, Phys. Rev. B **48**, 13115 (1993).
[28]G. Kresse and J. Furthmüller, Comput. Mater. Sci. **6**, 15 (1996).
[29]P. E. Blöchl, Phys. Rev. B **50**, 17953 (1994).
[30]J. P. Perdew, K. Burke, and M. Ernzerhof, Phys. Rev. Lett. **77**, 3865 (1996).
[31]M. Topsakal and S. Ciraci, Phys. Rev. B **81**, 024107 (2010).
[32]W. Tang, E. Sanville, and G. Henkelman, J. Phys.: Condens Matter **21**, 084204 (2009).
[33]L. Pisani, J. A. Chan, B. Montanari, and N. M. Harrison, Phys. Rev. B **75**, 064418 (2007).